SCIENTIFIC REPORTS

OPEN

SUBJECT AREAS:
TOPOLOGICAL INSULATORS
ELECTRONIC PROPERTIES AND MATERIALS
TWO-DIMENSIONAL MATERIALS

Received
2 July 2013

Accepted
22 October 2013

Published
6 November 2013

Correspondence and requests for materials should be addressed to J.X. (xia.jing@uci.edu)

* These authors contributed equally to this work.

Surface Hall Effect and Nonlocal Transport in SmB_6: Evidence for Surface Conduction

D. J. Kim*, S. Thomas*, T. Grant, J. Botimer, Z. Fisk & Jing Xia

Dept. of Physics and Astronomy, University of California, Irvine, California 92697, USA.

A topological insulator (TI) is an unusual quantum state in which the insulating bulk is topologically distinct from vacuum, resulting in a unique metallic surface that is robust against time-reversal invariant perturbations. The surface transport, however, remains difficult to isolate from the bulk conduction in most existing TI crystals (particularly Bi_2Se_3, Bi_2Te_3 and Sb_2Te_3) due to impurity caused bulk conduction. We report in large crystals of topological Kondo insulator (TKI) candidate material SmB_6 the thickness-independent surface Hall effects and non-local transport, which persist after various surface perturbations. These results serve as proof that at low temperatures SmB6 has a metallic surface that surrounds an insulating bulk, paving the way for transport studies of the surface state in this proposed TKI material.

Recently discovered[1–7] three-dimensional (3D) topological insulators (TI) have generated great excitement. Strong spin-orbit coupling in a TI gives rise to a non-trivial and robust conducting surface state[4,5], reminiscent of the edge channel[8,9] found in quantum Hall (QH)[10,11] and quantum spin Hall (QSH)[12,13] states. However, such surface transport properties have remained challenging to separate from residual bulk impurity conduction[14–17] despite rapid recent improvements[7,18–21], promoting us to search for TI materials with better bulk insulation. More importantly, most theoretical and experimental efforts to date have been dedicated to materials with the underlying physics of non-interacting electrons[1,4,5,12]. A big question thus concerns the role of electron interaction and competing orders in new TI materials with strong correlation, from which new types of topological phases are expected to emerge[4,5].

Recent seminal theoretical works[22,23] have predicted in the strongly correlated material SmB_6 the existence of a topological insulator phase: topological Kondo insulator (TKI). SmB_6 is a heavy fermion material first studied 40 years ago[24]. In SmB_6, highly renormalized f-electrons hybridize with conduction electrons and form a completely filled band of quasiparticles with a transport excitation gap Δ of about 40 Kelvin. However, its many exotic properties[25–27] still defy a satisfactory understanding within the framework of conventional insulators. One of these mysteries is the peculiar residual conduction at the lowest temperatures. Behaving electronically like an insulator at high temperatures, at low temperature its resistance mysteriously saturates: a curiosity that is usually attributed to the existence of density of states within the band gap. According to the recent TKI theory[22,23,28,29], the hybridization and odd parity wavefunction lead to strong spin-orbit coupling in SmB_6 and give rise to a topological surface state, which naturally explains the origin of the in-gap state and pinpoints its location to be on the surface of SmB_6. Our recent capacitance measurements on high quality SmB_6 crystals revealed intriguing anomalous capacitance effects[30] that could be explained by assuming the in-gap-states exist on the surface. In this paper we present evidence of thickness-independent surface Hall effect and nonlocal transport in high quality SmB_6 crystals of various geometries and from different growth batches. These results reveal in SmB_6 an insulating bulk and a conducting surface.

Results

Hall effect measurements were carried out in wedge-shaped SmB_6 crystals. As depicted in the inset in Fig. 1(a), the sample is placed in a perpendicular magnetic field $\vec{B}$ and current I flows between the two ends of the wedge. The Hall resistances $R_{xy} = V_{xy}/I$ are measured at different thicknesses d to distinguish between surface and bulk conduction. For bulk conduction $R_{xy}/B \propto 1/d$, while R_{xy}/B is d-independent if surface conduction dominates. In both cases, one can define a Hall coefficient $R_H = E_y/j_xB$ independent of B, where j_x is the current density (surface

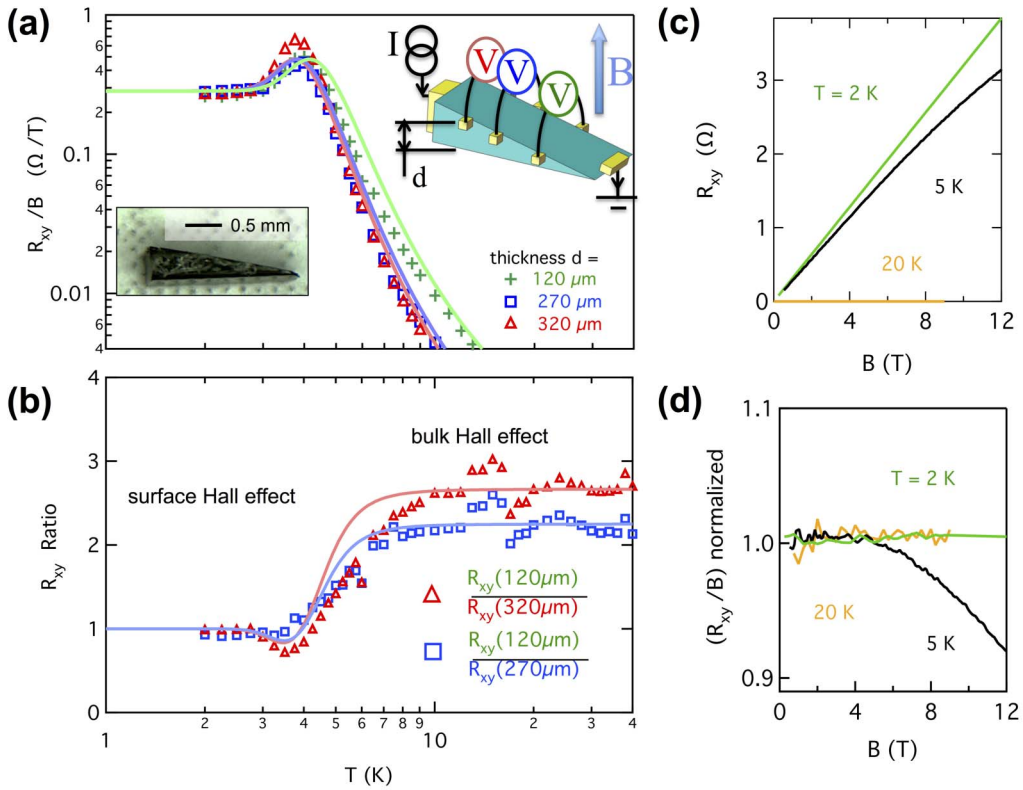

Figure 1 | Surface Hall effect. (a), Markers, Hall resistances R_{xy} divided by magnetic field B versus temperature T at three different thicknesses d in a wedge shaped sample *S1*. Lines are simulations using a two conduction channel model (see text). Left inset, picture of the crystal before wiring. Right inset, measurement schematic. (b), Markers, ratios between Hall resistances R_{xy} at different d, showing the transition from bulk to surface conduction as temperature is lowered. Lines are calculated from simulations as in (a). (c), R_{xy} versus B at various T for $d = 120$ μm, showing nonlinearity at around 5 K. (d), R_{xy}/B normalized to small field values to demonstrate the nonlinearity.

or bulk) and E_y is the transverse electric field. The Hall voltage V_{xy} is found to be linear with B (Fig. 1(c) (d)) at small fields at all temperatures, but becomes significantly nonlinear for larger fields around 5 K, indicating a temperature regime of multichannel conduction. At high (20 K) or low (2 K) temperatures, the extreme linearity of the Hall effect indicates single channel conduction, either from the bulk or surface. For the simplest case of one surface conduction channel (top and bottom surfaces combined) and one bulk channel with Hall coefficients R_{HS}, R_{HB} and resistivity ρ_S, ρ_B respectively, the Hall resistance R_{xy} at magnetic field B is $R_{xy} = \left[\left(R_{HS}\rho_B^2 + R_{HB}\rho_S^2 d\right)B + R_{HS}R_{HB}(R_{HS}d + R_{HB})B^3\right] / \left[(\rho_S d + \rho_B)^2 + (R_{HS}d + R_{HB})^2 B^2\right]$. Nonlinearity is expected at large B, but at small fields it simplifies to $R_{xy}/B = \left(R_{HS}\rho_B^2 + R_{HB}\rho_S^2 d\right) / (\rho_S d + \rho_B)^2$, which indeed gives thickness-independent $R_{xy}/B = R_{HS}$ if the surface channel dominates (i.e. $\rho_B \gg \rho_S d$). From $B < 1$ T data we extract the value R_{xy}/B at various temperatures T. Representative results in sample *S1* are plotted in Fig. 1(a) for $d = 120$, 270, and 320 μm respectively, showing clearly that while at high temperatures R_{xy}/B differ at different d, they converge to a same universal value of 0.3 Ω/T below 4 Kelvin, consistent with surface conduction. Since more than one surface channels may exist, as predicted by theory[28,29], it is difficult to quantitatively extract the surface carrier density and mobility at this stage. Replotting the Hall resistance ratios $R_{xy}(d_1)/R_{xy}(d_2)$ in Fig. 1(b), we found these ratios to be equal to d_2/d_1 at high T and become unity at low T, proving the crossover from 3D to 2D Hall effects when T is lowered. The temperature dependence is well described by a two-channel (bulk and surface) conduction model in which the bulk carrier density decreases exponentially with temperature with an activation gap $\Delta = 38$ K. Using this simple model, we could reproduce the curious "peak" in R_{xy}/B at 4 K (solid lines in Fig. 1(a)), which lacks[31] a good explanation until now. Low temperature surface-dominated conduction would also give rise to a longitudinal resistance R_{xx} that is independent of sample thickness, which we have demonstrated recently[32].

Surface dominated conduction could also be demonstrated at zero magnetic field with so-called "non-local" transport in the spirit of nonlocal transport experiments performed in QH[10,11] and QSH[12,13] states that have served as evidence[8,9] for the existence of the topological edge states that are one-dimensional analogues to the surface state in a TI. The highly metallic surface conduction in a TI would necessarily invalidate Ohm's law and introduce large nonlocal voltages, which we have indeed found in SmB_6 samples. Fig. 2(a) shows a schematic of the nonlocal measurement in sample *S4*. Current I_{16} flows between current leads 1 and 6 at the center on opposite faces of the crystal. Contacts 2 and 3 are located close to contact 1 for the detection of "local" voltage V_{23}. Contacts 4 and 5 are put near the sample edge far away from the current leads to detect "nonlocal" voltage V_{45}. As shown in the inset in Fig. 2(b), in the case of bulk conduction, current will concentrate in the bulk near the current leads 1 and 6, resulting in negligibly small nonlocal voltage ($V_{45} \ll V_{23}$). If surface conduction dominates, however, current will be forced to flow between contacts 1 and 6 via the surface, making V_{45} larger. Fig. 2(a) shows as a function of temperature the measured V_{45} and V_{23} divided by I_{16}, both agreeing qualitatively with our finite element simulations (Supplementary Information) incorporating the aforementioned simple model. The ratio V_{45}/V_{23} is replotted in Fig. 2(b). At low temperature, when surface conduction dominates, the nonlocal voltage V_{45} becomes large and even surpasses the local voltage V_{23}. Above $T = 5$ K, when bulk conduction dominates, the magnitude of V_{45}/V_{23} is very small. The negative sign of V_{45}/V_{23} is

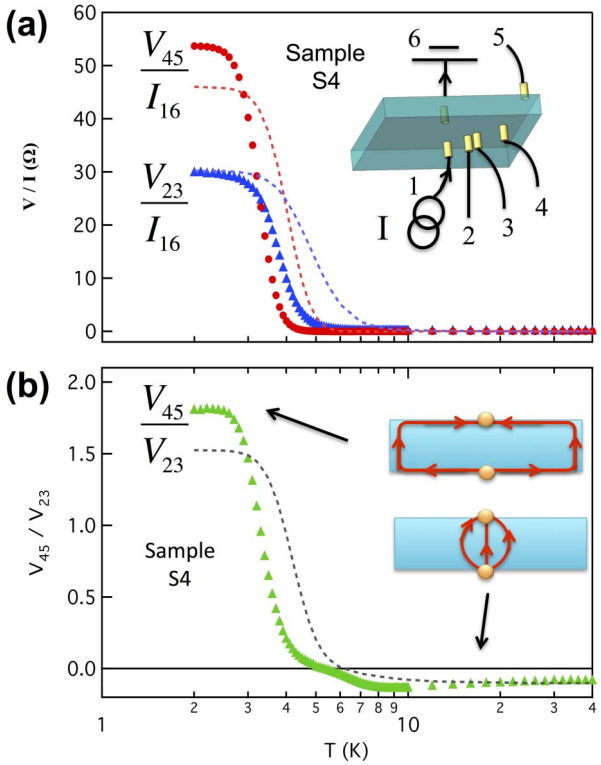

Figure 2 | Nonlocal transport due to surface conduction. (a), Markers, nonlocal resistance V_{45}/I_{16} and local resistance V_{23}/I_{16} versus temperature T. Dashed lines are finite element simulations. Inset is a schematic of the measurement configuration on sample *S4*. (b), Ratio between nonlocal and local voltages V_{45}/V_{23} versus T. Dashed lines are finite element simulations. Inset, cartoons for current distribution in sample cross-section for surface and bulk dominated conductions.

due to the small misalignment of contacts (Supplementary Information). The change of both magnitude and sign of V_{45}/V_{23} is reproduced by our simulation and highlights the distinction between high T bulk conduction and low T surface conduction.

An important aspect of TI is the topological protection of the surface state against time-reversal invariant perturbations. The robustness against perturbation distinguishes a topological surface state from "accidental" surface conduction[4,5]. We found that the above surface Hall effect and nonlocal transport are recurrent phenomena in various samples and persist after chemical and mechanical sample treatments. We have mechanically cut and scratched the surface of sample *S10* (Fig. 3 inset) and performed Hall measurements before and after surface abrasion. We found that the low temperature Hall resistance R_{xy}/B remained unchanged (Fig. 3(c)), indicating that the surface carrier density n_S was not affected by abrasion. The abrasion does reduce the surface mobility μ_S though, as reflected by the height of R_{xy}/B "peak" at $T = 4$ *K*, presumably due to greatly enhanced geometric roughness. As shown in Fig. 3 (a) (b), the surface dominated conduction persists after abrasion, as demonstrated by the thickness-independent Hall effect below 4 K.

Discussion

The experimental identification of thickness-independent surface Hall effect and nonlocal transport serve as strong evidence that SmB_6 has a metallic surface state surrounding an insulating bulk at low temperatures. The characterization of energetics of the surface state and hence direct tests of the topological nature, however, awaits future investigations using energy and spin resolved techniques like ARPES[2,3] and STM[33,34]. Recent ARPES[35–37], quantum oscillation[38] and STM measurements[39] have provided further evidence of surface conduction, as well as insights of the surface electronic structure. Recent transport measurements with doped SmB_6 samples[32] have demonstrated that the surface conduction persists after non-magnetic doping but is destroyed by magnetic doping, as expected from a

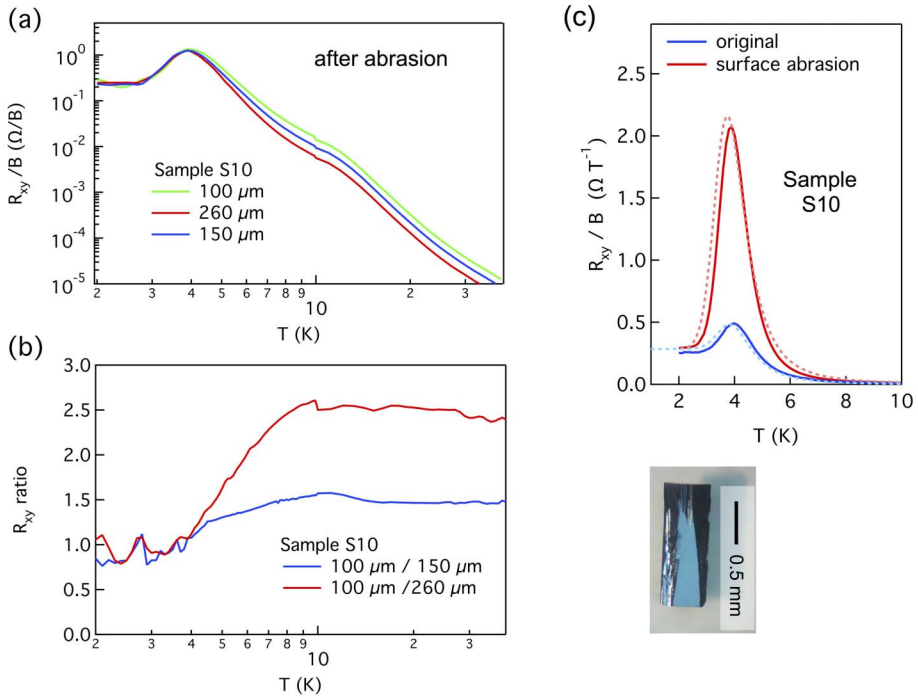

Figure 3 | Surface conduction after surface treatments. (a), Markers, Hall resistances R_{xy} divided by magnetic field B versus temperature T at three different thicknesses d in a wedge shaped sample *S10, after intentional chemical etching and cutting.* (b), Markers, ratios between Hall resistances R_{xy} at different d, showing the transition from bulk to surface conduction as temperature is lowered. (c), Solid lines, Hall resistance R_{xy} divided by magnetic field B versus temperature T, *before and after surface abrasion.* Dashed lines are simulations assuming abrasion *only* reduces the effective surface mobility μ_S. Inset, picture of sample S*10* during abrasion.

topological surface state protected by time-reversal-symmetry. Transport experiments[40] at lower temperatures have revealed the weak-anti-localization effect, which is expected from a spin-momentum-locked topological surface state. Unlike weakly interacting TI materials, the strong electron correlation in SmB_6 could give rise to exotic emergent phases[4,5] with exciting new physics.

Note added: During initial submission of the manuscript, we became aware of a related work[41] in which evidence for surface conduction was provided in a SmB_6 sample with contacts arranged in a unique configuration, and a point contact measurement[42] that excludes the possibility that the in-gap state is located in the bulk of SmB_6.

Methods

High quality SmB_6 crystals were grown using the aluminium flux method. The surfaces of these crystals were carefully etched using hydrochloric acid and then cleaned using solvents to remove possible oxide layer or aluminium residues. These crystals are then inspected using X-ray analysis to make sure SmB_6 is the only content. Samples used in the experiments were made from these crystals either by mechanical cleaving or polishing using polishing films containing diamond particles. The exposed surfaces are (100) planes. Gold and platinum wires are attached to the samples using micro spot welding and/or silver epoxy, with no discernable differences in measurements. Low frequency transport measurements were carried out in dilution fridges and helium cryostats using either standard low frequency (37 Hz) lock-in techniques with 50 *nA* excitation currents or with a resistance bridge.

1. Fu, L. & Kane, C. L. Topological insulators with inversion symmetry. *Phys. Rev. B.* **76**, 045302 (2007).
2. Hsieh, D. *et al.* A topological Dirac insulator in a quantum spin Hall phase. *Nature* **452**, 970–974 (2008).
3. Chen, Y. L. *et al.* Experimental realization of a three-dimensional topological insulator, Bi_2Te_3. *Science* **325**, 178–181 (2009).
4. Qi, X.-L. & Zhang, S.-C. Topological insulators and superconductors. *Rev. Mod. Phys.* **83**, 1057–1110 (2011).
5. Hasan, M. & Kane, C. Colloquium: Topological insulators. *Rev. Mod. Phys.* **82**, 3045–3067 (2010).
6. Roy, R. Topological phases and the quantum spin Hall effect in three dimensions. *Phys. Rev. B.* **79**, 195322 (2009).
7. Brune, C. *et al.* Quantum Hall effect from the topological surface states of strained bulk HgTe. *Phys. Rev. Lett.* **106**, 126803 (2011).
8. McEuen, P. *et al.* New resistivity for high-mobility quantum Hall conductors. *Phys. Rev. Lett.* **64**, 2062–2065 (1990).
9. Roth, A. *et al.* Nonlocal transport in the quantum spin Hall state. *Science* **325**, 294–297 (2009).
10. Klitzing von, K., DORDA, G. & Pepper, M. New method for high-accuracy determination of the fine-structure constant based on quantized Hall resistance. *Phys. Rev. Lett.* **45**, 494–497 (1980).
11. Tsui, D. C., Stormer, H. L. & Gossard, A. C. Two-dimensional magnetotransport in the extreme quantum limit. *Phys. Rev. Lett.* **48**, 1559–1562 (1982).
12. Bernevig, B. A., Hughes, T. L. & Zhang, S.-C. Quantum spin Hall effect and topological phase transition in HgTe quantum wells. *Science* **314**, 1757–1761 (2006).
13. Koenig, M. *et al.* Quantum spin hall insulator state in HgTe quantum wells. *Science* **318**, 766–770 (2007).
14. Peng, H. *et al.* Aharonov-Bohm interference in topological insulator nanoribbons. *Nat. Mater.* **9**, 225–229 (2009).
15. Checkelsky, J., Hor, Y., Cava, R. & Ong, N. Bulk band gap and surface state conduction observed in voltage-tuned crystals of the topological insulator Bi_2Se_3. *Phys. Rev. Lett.* **106**, 196801 (2011).
16. Analytis, J. G. *et al.* Two-dimensional surface state in the quantum limit of a topological insulator. *Nat. Phys.* **6**, 960–964 (2010).
17. Taskin, A. & Ando, Y. Quantum oscillations in a topological insulator $Bi_{1-x}Sb_x$. *Phys. Rev. B.* **80**, 085303 (2009).
18. Ren, Z., Taskin, A. A., Sasaki, S., Segawa, K. & Ando, Y. Large bulk resistivity and surface quantum oscillations in the topological insulator Bi_2Te_2Se. *Phys. Rev. B.* **82**, 241306 (2010).
19. Jia, S. *et al.* Low-carrier-concentration crystals of the topological insulator Bi_2Te_2Se. *Phys. Rev. B.* **84**, 235206 (2011).
20. Xiong, J. *et al.* Quantum oscillations in a topological insulator Bi_2Te_2Se with large bulk resistivity. *Physica E* **44**, 917–920 (2012).
21. Xiong, J. *et al.* High-field Shubnikov-de Haas oscillations in the topological insulator Bi_2Te_2Se. *Phys. Rev. B.* **86**, 045314 (2012).
22. Dzero, M., Sun, K., Galitski, V. & Coleman, P. Topological Kondo insulators. *Phys. Rev. Lett.* **104**, 106408 (2010).
23. Dzero, M., Sun, K., Coleman, P. & Galitski, V. Theory of topological Kondo insulators. *Phys. Rev. B.* **85**, 045130 (2012).
24. Menth, A., Buehler, E. & Geballe, T. Magnetic and semiconducting properties of SmB_6. *Phys. Rev. Lett.* **22**, 295–297 (1969).
25. Nickerson, J. *et al.* Physical properties of SmB_6. *Phys. Rev. B.* **3**, 2030–2042 (1971).
26. Barla, A. *et al.* High-pressure ground state of SmB_6: electronic conduction and long range magnetic order. *Phys. Rev. Lett.* **94**, 166401 (2005).
27. Derr, J. *et al.* From unconventional insulating behavior towards conventional magnetism in the intermediate-valence compound SmB_6. *Phys. Rev. B.* **77**, 193107 (2008).
28. Lu, F., Zhao, J., Weng, H., Fang, Z. & Dai, X. Correlated topological insulators with mixed valence. *Phys. Rev. Lett.* **110**, 096401 (2013).
29. Alexandrov, V., Dzero, M. & Coleman, P. Cubic topological Kondo insulators. *arXiv:1303.7224* (2013).
30. Kim, D., Grant, T. & Fisk, Z. Limit cycle and anomalous capacitance in the Kondo insulator SmB_6. *Phys. Rev. Lett.* **109**, 096601 (2012).
31. Cooley, J., Aronson, M., Fisk, Z. & Canfield, P. SmB_6: Kondo insulator or exotic metal? *Phys. Rev. Lett.* **74**, 1629–1632 (1995).
32. Kim, D. J., Xia, J. & Fisk, Z. Topological surface state in the Kondo insulator samarium hexaboride. *arXiv:1307.0448* (2013).
33. Alpichshev, Z. *et al.* STM imaging of electronic waves on the surface of Bi_2Te_3: topologically protected surface states and hexagonal warping effects. *Phys. Rev. Lett.* **104** (2010).
34. Roushan, P. *et al.* Topological surface states protected from backscattering by chiral spin texture. *Nature* **460**, 1106–1109 (2009).
35. Neupane, M. *et al.* Surface electronic structure of a topological Kondo insulator candidate SmB_6: insights from high-resolution ARPES. *arXiv:1306.3678* (2013).
36. Jiang, J. *et al.* Observation of in-gap surface states in the Kondo insulator SmB_6 by photoemission. *arXiv:1306.5664* (2013).
37. Xu, N. *et al.* Surface and bulk electronic structure of the strongly correlated system SmB_6 and implications for a topological Kondo insulator. *arXiv:1306.3678* (2013).
38. Li, G. *et al.* Quantum oscillations in Kondo insulator SmB_6. *arXiv:1306.5221* (2013).
39. Yee, M. M. *et al.* Imaging the Kondo insulating gap on SmB_6. *arXiv:1308.1085* (2013).
40. Thomas, S. *et al.* Weak antilocalization and linear magnetoresistance in the surface state of SmB. *arXiv:1307.4133* (2013).
41. Wolgast, S. *et al.* Low temperature surface conduction in the Kondo insulator SmB_6. *arXiv:1211.5104* (2012).
42. Zhang, X. *et al.* Hybridization, inter-ion correlation, and surface states in the Kondo insulator SmB_6. *Phys. Rev. X* **3**, 011011 (2013).

Acknowledgments

We thank T.H. Geballe and A. Kapitulnik for useful discussions. This work was supported by UC Irvine CORCL Grant MIIG-2011-12-8, Sloan Research Fellowship #BR2013-116 (J. X.). Crystal growth was supported by NSF grant #DMR-0801253.

Author contributions

J.X. conceived the project. D.J.K., T.G. and Z.F. grew the crystals. D.J.K., S.T., J.B., and J.X. fabricated the samples and performed the measurements. T.G. performed X-ray analysis of the crystals. S.T. and J.X. performed the simulations. All authors analysed the data and wrote the manuscript.

Additional information

Supplementary information accompanies this paper at http://www.nature.com/scientificreports

Competing financial interests: The authors declare no competing financial interests.

How to cite this article: Kim, D.J. *et al.* Surface Hall Effect and Nonlocal Transport in SmB_6: Evidence for Surface Conduction. *Sci. Rep.* **3**, 3150; DOI:10.1038/srep03150 (2013).